

# Bicoherence and Zonal Flow at the L–H Transition in TJ-II

B.Ph. van Milligen<sup>1</sup>, T. Estrada<sup>1</sup>, C. Hidalgo<sup>1</sup>, T. Happel<sup>2</sup>, E. Ascasíbar<sup>1</sup>

<sup>1</sup>*Asociación EURATOM-CIEMAT para Fusión,  
Avda. Complutense 40, 28040 Madrid, Spain and*

<sup>2</sup>*Max Planck Institut für Plasmaphysik,  
Association Euratom-IPP, 85748 Garching, Germany*

(Dated: April 11, 2019)

## Abstract

The interaction between zonal flow oscillations and turbulence is studied using Doppler reflectometry measurements at the TJ-II stellarator. By scanning the tilt angle of the probing beam, different values of the perpendicular wave numbers are probed at the reflection layer. In this way, the zonal flow – turbulence interaction can be studied with (a) spatial, (b) temporal, and (c) wavenumber resolution for the first time in any magnetic confinement fusion device.

We report measurements of the auto-bicoherence and cross bicoherence of both the raw reflectometry signal and the processed perpendicular velocity and turbulence amplitude, across the Low to High (L–H) confinement transition at TJ-II. We examine both fast transitions and slow transitions characterized by an intermediate (I) phase. The bicoherence, understood to reflect the non-linear coupling between the perpendicular velocity (zonal flow) and turbulence amplitude, is significantly enhanced in a time window of several tens of ms around the time of the L–H transition. It is found to peak at a specific radial position (slightly inward from the radial electric field shear layer in H mode), and is associated with a specific perpendicular wave number ( $k_{\perp} \simeq 6 - 12 \text{ cm}^{-1}$ ). In all cases, the bicoherence is due to the interaction between high frequencies and a rather low frequency, as expected for a zonal flow.

The Low to High confinement (L–H) transition at the TJ-II stellarator is a “soft” transition in the sense that the confinement improvement factor is small, and yet it possesses the typical features of any H-mode (rapid drop of  $H_\alpha$  emission, reduction of fluctuation amplitudes, formation of a sheared flow layer, ELM-like bursts) [1–4]. In the four years since the first observation of the H-mode at TJ-II, many experiments have been performed to explore its features.

A common explanation for the L–H transition involves the generation of a zonal flow in a narrow radial region of the plasma near its edge. The zonal flow would be driven by turbulence via the Reynolds Stress mechanism in a strong pressure gradient region [5]. The growth of the (fluctuating) zonal flow then leads to the suppression of turbulence, creating a transport barrier, and the subsequent establishment of a steady state sheared flow with associated radial electric field that maintains the barrier [6–8]. The detailed observation of this sequence of events is a challenge.

Due to the temporal and spatial scales involved in the L–H transition physics, specific experimental techniques are required to investigate the turbulence and flow dynamics [2]. At TJ-II, a two-channel Doppler reflectometer is available, allowing the simultaneous measurement of the perpendicular plasma velocity and density fluctuations at two radial positions, with good spatial and temporal resolution [9]. In addition, the Doppler reflectometer offers the possibility to probe different turbulence scales (wave vectors) by steering the probing beam [10, 11].

**Experimental setup** – The TJ-II vacuum magnetic geometry is completely determined by the currents flowing in four external coil sets. Three independent numbers, proportional to the coil currents, are compounded into a label to identify each configuration [12]. At TJ-II, the normalized pressure  $\langle\beta\rangle$  is generally low, even in discharges with Neutral Beam Injection (NBI), and currents flowing inside the plasma are generally quite small (unless explicitly driven), so that the actual magnetic configuration and the rotational transform  $\iota/2\pi$  are typically rather close to the vacuum magnetic configuration [13]. Here we focus on three magnetic configurations: 100\_50\_65 (having  $\iota(0)/2\pi = 1.613$ ,  $\iota(a)/2\pi = 1.704$ ), 101\_42\_64 ( $\iota(0)/2\pi = 1.534$ ,  $\iota(a)/2\pi = 1.630$ ), and 100\_35\_61 ( $\iota(0)/2\pi = 1.457$ ,  $\iota(a)/2\pi = 1.553$ ).

The experiments have been carried out in pure NBI heated plasmas (line averaged plasma density  $\langle n_e \rangle = 2 - 4 \times 10^{19} \text{ m}^{-3}$ , central electron temperature  $T_e = 300 - 400 \text{ eV}$ ). The NBI input heating power is kept constant at about 500 kW during the discharge but the fraction

of NBI absorbed power – taking into account shine through, CX and ion losses, as estimated using the FAFNER2 code [14] – increases from 55 to 70% as the plasma density rises.

In this work, we consider two different L–H transition scenarios. Standard or *fast* L–H transitions are observed in the magnetic configuration having  $\iota(a)/2\pi = 1.630$  [10], while *slow* transitions are observed in the configuration having  $\iota(a)/2\pi = 1.553$  and a low order rational ( $3/2$ ) at  $\rho = r/a \simeq 0.72$ . In the latter configuration, the so-called intermediate phase (I), characterized by a predator-prey type interaction between turbulence and flows, appears between the L and H phases [15, 16], which has also been seen in models [17, 18] and on other devices [19, 20]. In both scenarios, spatiotemporal and scale resolved Doppler reflectometry measurements were performed in series of repetitive discharges [10, 11].

**Doppler reflectometry** – In Doppler reflectometry, a finite tilt angle is purposely introduced between the incident probing beam and the normal to the reflecting cut-off layer, and the Bragg back-scattered signal is measured [21]. The amplitude of the recorded signal,  $A$ , is a measure of the intensity of the density fluctuations,  $\tilde{n}$ . By scanning the tilt angle of the probing beam, different perpendicular wave numbers are probed, thus allowing scale-resolved turbulence measurements. Furthermore, as the plasma rotates in the reflecting plane (flux surface), the scattered signal experiences a Doppler shift. The size of this shift is directly proportional to the rotation velocity of the plasma turbulence perpendicular to the magnetic field lines,  $v_\perp$ , and therefore to the plasma background  $E \times B$  velocity, provided the latter dominates over the phase velocity of density fluctuations (cf. [2]). Using the analysis method reported in [22],  $v_\perp$  can be determined with high temporal and spatial resolution. Doppler reflectometer signals are recorded at a sampling rate of 10 MHz.

The relation between zonal flow growth, involving an interaction between high frequencies associated with drift wave turbulence and low frequencies associated with the zonal flow, and the cross bispectrum was elucidated in [23]. Probing zonal flow dynamics therefore requires measuring the cross bispectrum between the radial and poloidal  $E \times B$  velocities of high-frequency drift waves and the low-frequency zonal flow. As such measurements are quite difficult to perform in the plasma interior, the bicoherence is often calculated using density fluctuations only, which complicates the interpretation of the results. However, Doppler reflectometry allows the measurement of the turbulence fluctuation amplitude  $\tilde{n}$  as well as the fluctuating perpendicular flow  $\tilde{v}_\perp$ , both with good temporal and spatial resolution, making the two main quantities involved in zonal flow dynamics accessible experimentally.

In this work, we consider the complex amplitude Doppler reflectometry signal,  $Ae^{i\phi} = (A \cos \phi, A \sin \phi)$ , which contains information of both the perpendicular flow,  $\tilde{v}_\perp = d\tilde{\phi}/dt$ , and the density turbulence,  $\tilde{n} \propto \tilde{A}$ .

**Bicoherence analysis** – The cross bicoherence of two signals  $f(t)$  and  $g(t)$  is defined as [24]

$$b_{fg}^2(\omega_1, \omega_2) = \frac{\langle |\hat{f}(\omega_1)\hat{f}(\omega_2)\hat{g}^*(\omega_1 + \omega_2)|^2 \rangle}{\langle |\hat{f}(\omega_1)\hat{f}(\omega_2)|^2 \rangle \langle |\hat{g}(\omega_1 + \omega_2)|^2 \rangle},$$

where  $\hat{f}(\omega)$  is the Fourier transform of  $f(t)$ , a star indicates the complex conjugate, and the angular brackets refer to an average over equivalent realizations. In practice, the equivalent realizations are successive time sections, assuming the system is in steady state. The value of  $b^2$  is bounded between 0 and 1, so that a high value indicates wave-wave coupling between the two base frequencies  $\omega_1$  and  $\omega_2$  and their sum frequency,  $\omega_1 + \omega_2$ . The auto-bicoherence is  $b_f^2 = b_{ff}^2$ .

We also report the “summed bicoherence”, defined as  $b_{\text{sum}}^2(\omega) = \langle b^2(\omega_1, \omega_2) \rangle_{\omega_1 + \omega_2 = \omega}$ , and the “total bicoherence”, defined as  $b_{\text{total}}^2 = \langle b^2(\omega_1, \omega_2) \rangle_{\omega_1, \omega_2}$ . Since the bicoherence itself is normalised between 0 and 1, the value of the summed and total bicoherence is also limited to this range. Even so, their value depends on the frequency resolution used to perform the calculations, a sharp spike in  $b^2(\omega_1, \omega_2)$  (a delta function) contributing to the summed bicoherence in proportion to the area in  $\omega_1 - \omega_2$  space occupied by a frequency grid element. Thus, the summed and total bicoherence are useful quantities to summarise the data, but their values should not be assigned any absolute meaning, since they are dependent on the details of the analysis procedure.

To judge the relevance of a bicoherence value, it is compared to the expectation value of the bicoherence under the assumption that the signal is uncorrelated random noise (called the “statistical error level”,  $\epsilon$ ) [25].

Computing the auto-bicoherence for the complex Doppler reflectometer data around the time of the L–H transition, one typically obtains results such as those shown in Fig. 1. The auto-bicoherence is very significant, as the value is some two orders of magnitude above the noise level. The auto-bicoherence is concentrated along the line  $f_2 \simeq -f_1/2$  (the ‘first harmonics’ line),  $f_2 \simeq f_1$  (interaction with a very small difference frequency), and also at  $f_2 \simeq 0$ . These are indications that high frequencies  $f_a, f_b$  of the order of 1–2 MHz are interacting via a very small difference frequency  $f_c = f_a - f_b$  (or harmonics  $f_c = 2f_a - f_b$ )

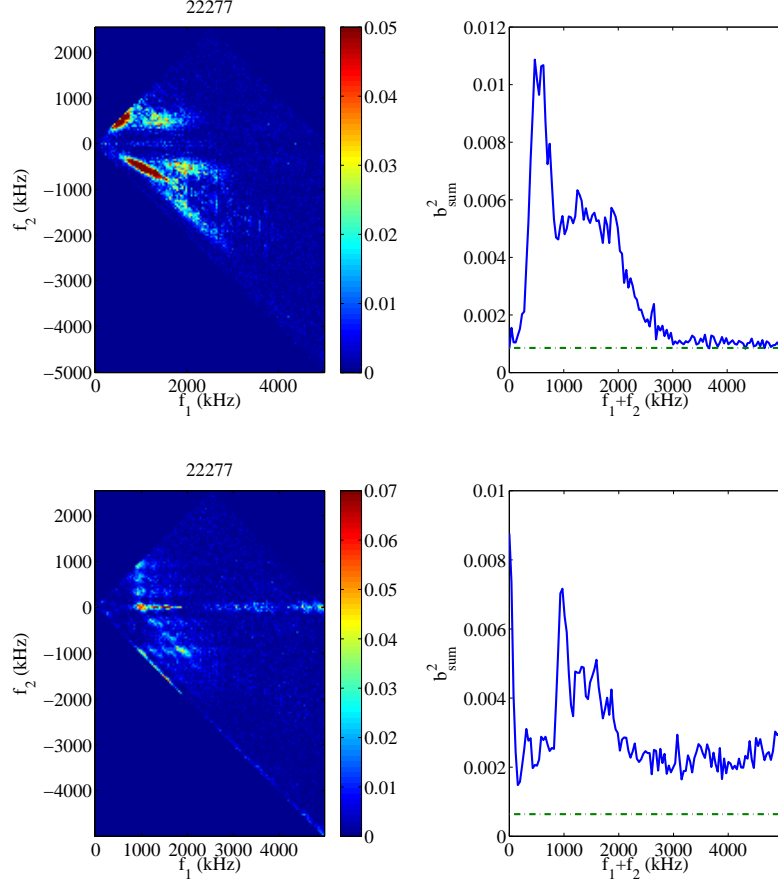


FIG. 1: Discharge 22277. Configuration with  $\iota(a)/2\pi = 1.704$ . Top: Mean auto-bicoherence and mean summed auto-bicoherence of complex Doppler reflectometry channel 1. Bottom: Cross bicoherence between  $\tilde{v}_\perp$  and  $\tilde{n}$  (Doppler reflectometry channel 1) during the L–H transition ( $1100 < t < 1130$  ms,  $t_{L-H} = 1116$  ms). The dashed line indicates the noise level.

such that  $|f_c| \ll |f_a|, |f_b|$ . Frequencies above 1 MHz are not commonly observed in this context due to technical limitations; however, note that similar results were obtained at DIII-D [26].

To facilitate the interpretation of the auto-bicoherence, Fig. 1 also shows the cross bicoherence between  $\tilde{v}_\perp$  and  $\tilde{n}$  for the same discharge. Here, significant coupling is limited mainly to the lines  $f_2 \simeq 0$  and  $f_2 \simeq \pm f_1$ , indicating an interaction between two very similar frequencies  $f_a, f_b$ , interacting via a very small difference frequency  $f_c = f_a - f_b$  such that  $|f_c| \ll |f_a|, |f_b|$ , while harmonics are weak. This is in fact what one would expect for the interaction between a zonal flow and turbulence [23, 27]. The small frequency of the triplet

is at or below frequency resolution (50 kHz), whereas the two high frequencies are in the range from 1 to 2 MHz. The fact that the cross bicoherence graph shows linear structures, while the auto-bicoherence exhibits additional harmonic structures, is a clear indication that the physical interaction primarily involves  $\tilde{v}_\perp$  and  $\tilde{n}$ . Hence, the cross bicoherence between  $\tilde{v}_\perp$  and  $\tilde{n}$  carries the largest physical significance, while the auto-bicoherence of the complex Doppler reflectometry signal, easier to compute and yielding larger bicoherence values, can be used as a generic proxy to study the spatiotemporal evolution of the total bicoherence.

**The fast L–H transition** – To study the radial behavior of the bicoherence across the fast L–H transition, we have analyzed a series of 25 discharges in the same magnetic configuration ( $\iota(a)/2\pi = 1.630$ ). See Ref. [10] for more details about this series of discharges. The Doppler reflectometer probing frequency and tilt angle were varied on a shot to shot basis, and correspondingly the radial position of the reflecting layer and the wave number  $k_\perp$ . Results are shown in Fig. 2. In the top figure, the bicoherence values are averaged over the available  $k_\perp$  values to display the mean behavior of the bicoherence versus  $\rho$  and time, while in the bottom figure, the bicoherence values are averaged over the available  $\rho$  values to display the mean behavior of the bicoherence versus  $k_\perp$  and time. It is seen that the bicoherence appears  $\sim 20 - 30$  ms before the L–H transition at a specific radius ( $\rho \lesssim 0.8$ ) and that specific perpendicular wave numbers are involved ( $k_\perp \simeq 8 - 11 \text{ cm}^{-1}$ ). The bicoherence persists until about  $10 - 20$  ms after the L–H transition.

Both the position of the reflecting layer and the wavenumber change as a function of time across the transition due to the evolving density profile. The values indicated on the vertical graph axes correspond to the situation in H-mode. In L-mode,  $\rho$  is smaller by about 0.1 at small values of  $\rho$  and by 0.025 at large values of  $\rho$  with respect to the indicated values [10], while  $k_\perp$  is smaller by less than 5%.

It should be noted that turbulence is reduced at all scales, but most in intermediate scales,  $k_\perp \simeq 7 - 11 \text{ cm}^{-1}$ , as reported in earlier work [10]. After the transition, the radial electric field shear layer is located at  $\rho \sim 0.83$ , somewhat outward from the position of the maximum observed bicoherence values.

**The slow L–I–H transition** – Fig. 3 shows the auto-bicoherence for a different series of discharges in the configuration with  $\iota(a)/2\pi = 1.553$ . The elaboration of this figure is equivalent to that of Fig. 2. The mean line average density at the L–H transition is about 50% lower than with the previous configuration. Another difference with the previous result

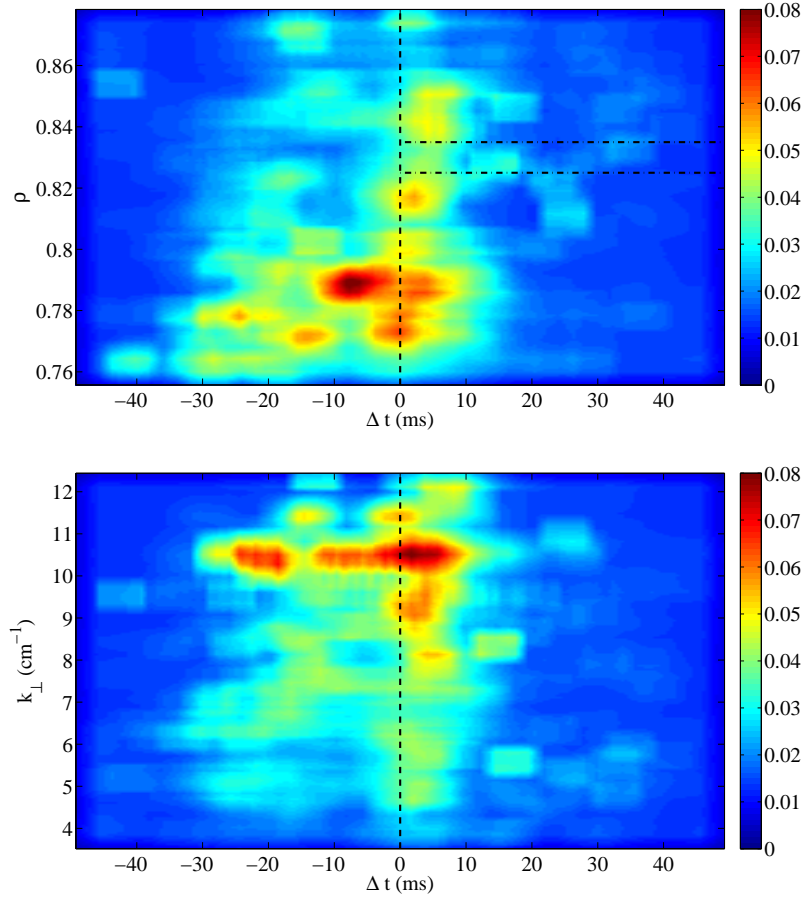


FIG. 2: Series of 25 discharges in the configuration with  $\iota(a)/2\pi = 1.630$ . Total auto-bicoherence of complex Doppler reflectometry data. Top: auto-bicoherence vs. time and normalized radius,  $\rho$ . Bottom: auto-bicoherence vs. time and  $k_{\perp}$ . Radii and  $k_{\perp}$  values correspond to the H-mode phase. The vertical dashed line indicates the L-H transition; the horizontal dashed lines indicate the approximate position of the  $E_r$  shear layer in the H phase. The statistical error level is about 0.006.

is that in these discharges, the transition at  $\Delta t = 0$  is not into the H-mode, but rather into the intermediate (I) phase between the L-mode ( $\Delta t < 0$ ) and the H-mode (starting much later). We conjecture that this situation is due to a weaker zonal flow, incapable of producing the final transition into the H phase. This would be consistent with the observation of predator-prey type behaviour, reported elsewhere [11], and associated with wave numbers in the range  $k_{\perp} \simeq 6 - 12 \text{ cm}^{-1}$ . The location of the auto-bicoherence peak appears to be somewhat further inward than in the previous section ( $\rho < 0.76$ ).

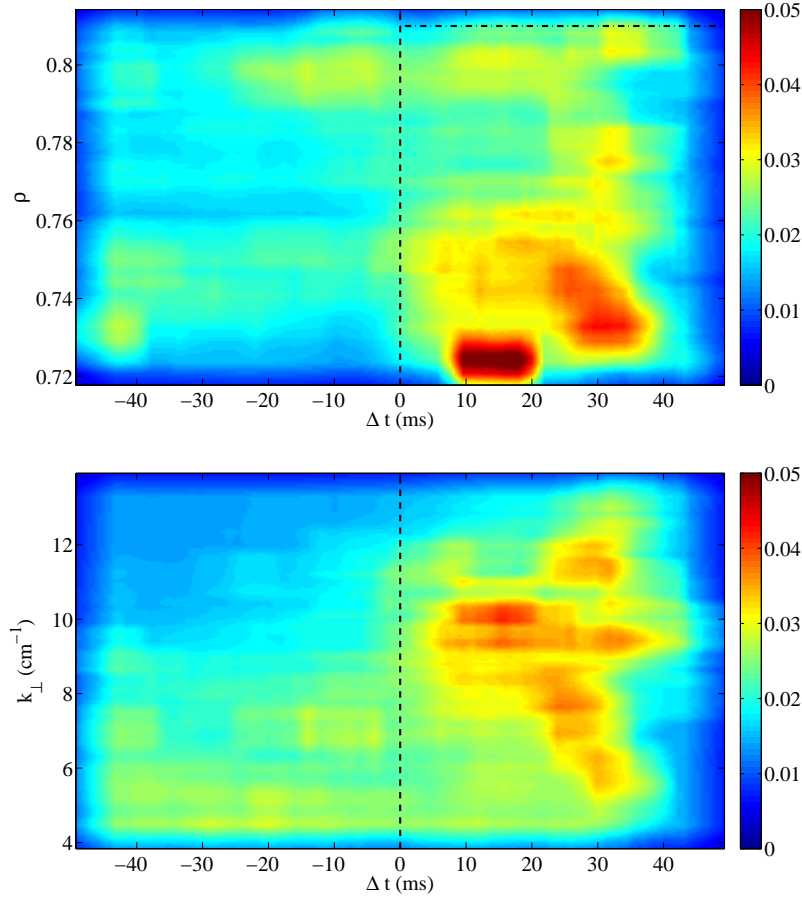


FIG. 3: Series of 26 discharges in configuration with  $\iota(a)/2\pi = 1.553$ . Total auto-bicoherence of complex Doppler reflectometry data. Top: auto-bicoherence vs. time and normalized radius,  $\rho$ . Bottom: auto-bicoherence vs. time and  $k_{\perp}$ . Radii and  $k_{\perp}$  values correspond to the H-mode phase. The vertical dashed line indicates the L–H transition; the horizontal dashed line indicates the approximate position of the  $E_r$  shear layer in the I phase. The statistical error level is about 0.006.

**Discussion and conclusions** – In this work, we have used Doppler reflectometry measurements to show how the bicoherence evolves across the L–H transition at TJ-II. It is the first time that turbulent fluctuation amplitudes and perpendicular (zonal) flow oscillations and their non-linear interactions have been observed simultaneously in the region of the plasma where the transport barrier of the L–H transition forms. While we have explored different magnetic configurations, the observations do not appear to depend very sensitively on the magnetic configuration. A surprisingly clear picture emerges that is consistent with



established ideas about the interaction between zonal flows and turbulence [28] in the important formation phase of the H-mode transport barrier.

In the case of the fast L-H transition, we have shown that the auto-bicoherence of the Doppler reflectometer signal is significant in a time window with a length of several tens of ms around the L-H transition time, at a particular radial position ( $\rho \lesssim 0.8$ , inward from the radial electric field shear layer in H mode), and that a specific range of perpendicular wave numbers is involved ( $k_{\perp} \simeq 8 - 11 \text{ cm}^{-1}$ ). Here,  $\rho_s = \sqrt{2m_i T_e}/eB = 0.1 - 0.2 \text{ cm}$ , so that this range corresponds to  $k_{\perp} \rho_s = 0.8 - 2$ .

A similar analysis in another set of discharges corresponding to a different magnetic configuration, in which the transition was characterized by an intermediate phase separating the L and H phases, the bicoherence appeared only after the L-I transition was made, and lasted several tens of ms afterward into the I phase. The perpendicular wave numbers involved ( $k_{\perp} \simeq 6 - 12 \text{ cm}^{-1}$ ) were very similar to the previous case, while the radial location of the bicoherence peak was somewhat further inward ( $\rho < 0.76$ ).

In both cases, the auto-bicoherence was due to high frequencies (of the order of 1–2 MHz) interacting with rather low frequencies ( $< 50 \text{ kHz}$ ), as expected for a zonal flow [18]. With the available data, it is not feasible to clearly resolve the low frequency component.

Putting these results into context, we note that this is the first time wave number resolved bicoherence during L-H transitions is reported. This important result indicates which spatial scales are important in the zonal flow coupling producing the L-H transition.

**Acknowledgements** – The authors would like to express their gratitude for continued support by the TJ-II team. Research sponsored in part by DGICYT of Spain under project Nrs. ENE2009-07247 and ENE2010-18409.

- 
- [1] F. Tabarés, M. Ochando, F. Medina, D. Tafalla, J. Ferreira, E. Ascasíbar, R. Balbín, T. Estrada, C. Fuentes, I. García-Cortés, et al., Plasma Phys. Control. Fusion **50**, 124051 (2008).
  - [2] T. Estrada, T. Happel, L. Eliseev, D. López-Bruna, E. Ascasíbar, E. Blanco, L. Cupido, J. Fontdecaba, C. Hidalgo, R. Jiménez-Gómez, et al., Plasma Phys. Control. Fusion **51**, 124015 (2009).

- [3] J. Sánchez, M. Acedo, A. Alonso, J. Alonso, P. Alvarez, E. Ascasíbar, A. Baciero, R. Balbín, L. Barrera, E. Blanco, et al., Nucl. Fusion **49**, 104018 (2009).
- [4] T. Estrada, E. Ascasíbar, T. Happel, C. Hidalgo, E. Blanco, R. Jiménez-Gómez, M. Liniers, D. López-Bruna, F. Tabarés, and D. Tafalla, Contrib. Plasma Phys. **50**, 501 (2010).
- [5] P. Manz, M. Ramisch, and U. Stroth, Phys. Rev. Lett. **103**, 165004 (2009).
- [6] K. Burrell, Phys. Plasmas **4**, 1499 (1997).
- [7] P. Diamond, S.-I. Itoh, K. Itoh, and T. Hahm, Plasma Phys. Control. Fusion **47**, R35 (2005).
- [8] F. Wagner, Plasma Phys. Control. Fusion **49**, B1 (2007).
- [9] T. Happel, T. Estrada, E. Blanco, V. Tribaldos, A. Cappa, and A. Bustos, Rev. Sci. Instrum. **80**, 073502 (2009).
- [10] T. Happel, T. Estrada, E. Blanco, C. Hidalgo, G. Conway, U. Stroth, and the TJ-II Team, Phys. Plasmas **18**, 102302 (2011).
- [11] T. Estrada, E. Ascasíbar, E. Blanco, A. Cappa, P. Diamond, T. Happel, C. Hidalgo, M. Liniers, B. van Milligen, I. Pastor, et al., Plasma Phys. Control. Fusion **54** (2012).
- [12] B. van Milligen, M. Pedrosa, C. Hidalgo, B. Carreras, T. Estrada, J. Alonso, J. de Pablos, A. Melnikov, L. Krupnik, L. Eliseev, et al., Nucl. Fusion **51**, 113002 (2011).
- [13] B. van Milligen, T. Estrada, E. Ascasíbar, D. Tafalla, D. López-Bruna, A. López-Fraguas, J. Jiménez, I. García-Cortés, A. Dinklage, R. Fischer, et al., Rev. Sci. Instrum. **82**, 073503 (2011).
- [14] M. Rodríguez-Pascual, J. Guasp, F. Castejón Magaña, A. Rubio-Montero, I. Martón Llorente, and R. Mayo García, IEEE Trans. Plasma Sc. **38**, 2102 (2010).
- [15] T. Estrada, T. Happel, C. Hidalgo, E. Ascasíbar, and E. Blanco, Eur. Phys. Lett. **92**, 35001 (2010).
- [16] T. Estrada, C. Hidalgo, T. Happel, and P. Diamond, Phys. Rev. Lett. **107**, 245004 (2011).
- [17] E.-J. Kim and P. Diamond, Phys. Plasmas **10**, 1698 (2003).
- [18] K. Miki, P. Diamond, Ö. Gürçan, G. Tynan, T. Estrada, L. Schmitz, and G. Xu, Phys. Plasmas **19**, 092306 (2012).
- [19] G. Conway, C. Angioni, F. Ryter, P. Sauter, J. Vicente, and the ASDEX Upgrade Team, Phys. Rev. Lett. **106**, 065001 (2011).
- [20] L. Schmitz, L. Zeng, T. Rhodes, J. Hillesheim, E. Doyle, R. Groebner, W. Peebles, K. Burrell, and G. Wang, Phys. Rev. Lett. **108**, 155002 (2012).

- [21] M. Hirsch, E. Holzhauser, J. Baldzuhn, B. Kurzan, and B. Scott, Plasma Phys. Control. Fusion **43**, 1641 (2001).
- [22] T. Estrada, T. Happel, and E. Blanco, Nucl. Fusion **52**, 082002 (2012).
- [23] P. Diamond, M. Rosenbluth, E. Sánchez, C. Hidalgo, B. van Milligen, T. Estrada, B. Brañas, M. Hirsch, H. Hartfuss, and B. Carreras, Phys. Rev. Lett. **84**, 4842 (2000).
- [24] B. van Milligen, T. Kalhoff, M. Pedrosa, and C. Hidalgo, Nucl. Fusion **48**, 115003 (2008).
- [25] B. van Milligen, E. Sánchez, T. Estrada, C. Hidalgo, B. Brañas, B. Carreras, and L. García, Phys. Plasmas **2**, 3017 (1995).
- [26] R. Moyer, G. Tynan, C. Holland, and M. Burin, Phys. Rev. Lett. **87**, 135001 (2001).
- [27] Y. Nagashima, K. Itoh, S.-I. Itoh, A. Fujisawa, K. Hoshino, Y. Takase, M. Yagi, A. Ejiri, K. Ida, K. Shinohara, et al., Plasma Phys. Control. Fusion **48**, S1 (2006).
- [28] A. Fujisawa, A. Shimizu, H. Nakano, S. Ohshima, K. Itoh, Y. Nagashima, S.-I. Itoh, H. Iguchi, Y. Yoshimura, T. Minami, et al., Plasma Phys. Control. Fusion **49**, 211 (2007).